JOURNAL OF GUIDANCE, CONTROL, AND DYNAMICS
Vol. 29, No. 3, May–June 2006

Free-Wing Unmanned Aerial Vehicle as a Microgravity Facility

Alwin M. Kraeger*
Delft University of Technology, 2629 HS Delft, The Netherlands

A conceptual study is presented on the dynamics of a proposed unmanned aerial vehicle (UAV), which is designed as a testbed for studying the influence of micro- (or partial) gravity on various biological or physical phenomena. The design option of a torque-controlled wing, free to rotate about a spanwise axis, is evaluated in terms of gust sensitivity and automatic settling at a certain *g*-setpoint. The complete set of nonlinear equations of motion of such a free-wing UAV are derived using Lagrange's equations. A linear aerodynamic model of the UAV is used to investigate its flight dynamics, gust sensitivity, and ability to fly micro- and partial gravity flights. Comparison to a similar fixed-wing UAV shows considerably decreased gust sensitivity.

Nomenclature

C_m = dimensionless moment coefficient about the center of gravity of the fuselage
c = cosine
$\bar{c}$ = mean aerodynamic chord
F = generalized force
$\boldsymbol{f}$ = position of the fuselage center of mass
g = Earth's gravitational acceleration
H = transfer function
$\boldsymbol{h}$ = position of the intersection of the hinge lines of both wing halves
L = Lagrangian function
$\boldsymbol{lw}$ = position of the left wing half center of mass
M = moment
m = mass
n = load factor
p = angular velocity component of the fuselage along the x_f axis
q = angular velocity component of the fuselage along the y_f axis
$\boldsymbol{q}$ = column vector of generalized coordinates
$\boldsymbol{R}$ = transformation matrix between two reference frames
r = angular velocity component of the fuselage along the z_f axis
$\boldsymbol{rw}$ = position of the right wing half center of mass
S = power spectral density
s = angular velocity component of the wing halves along their hinge axes
s = sine
T = kinetic energy
t = tangent
t = time
u = geodetic velocity component of the center of mass of the fuselage along the x_f axis
V = potential energy
v = geodetic velocity component of the center of mass of the fuselage along the y_f axis
$\boldsymbol{v}$ = velocity
w = geodetic velocity component of the center of mass of the fuselage along the z_f axis
$\boldsymbol{w}$ = column vector denoting the center of mass of the wing halves in wing fixed axes
x = in combination with index: x coordinate of the element indicated by the index; without index: x-position coordinate of the fuselage center of mass in geodetic reference frame
y = in combination with index: y coordinate of the element indicated by the index; without index: y-position coordinate of the fuselage center of mass in geodetic reference frame
z = in combination with index: z coordinate of the element indicated by the index; without index: z position coordinate of the fuselage center of mass in geodetic reference frame
α = angle of attack
Γ = hinge axis dihedral angle
γ = flight path angle
δ_e = elevator deflection
δW = increment in virtual work
δq = incremental virtual displacement
δ_w = angular deflection of the wing halves
ζ = damping
θ = pitch angle
Λ = hinge axis sweepback angle
σ = standard deviation
φ = roll angle
ψ = heading angle
$\boldsymbol{\Omega}$ = skew symmetric matrix
$\boldsymbol{\omega}$ = column vector of (angular) velocity components
ω_0 = undamped natural frequency

Subscripts and Superscripts

ac = aerodynamic center
cg = center of gravity
f = fuselage
g = geodetic
h = hinge
lw = left wing half
m = intersection of hinge axes
rw = right wing half
tot = total
w = wing
0 = initial

I. Introduction

IN a wide range of scientific disciplines, experiments are performed under microgravity conditions to investigate the influence of gravity on systems. These investigations range from physiological experiments on the human body to experiments at the level of

Presented as Paper 2000-4203 at the AIAA Atmospheric Flight Mechanics Conference, Denver, CO, 14–17 August 2000; received 6 May 2003; revision received 21 May 2004; accepted for publication 2 September 2004.

*Research Assistant, Faculty of Aerospace Engineering, Kluyverweg 1, Delft; A.M.Kraeger@lr.tudelft.nl.

molecules in fluids. The required duration of the microgravity periods for these experiments varies from seconds to days or even years.

Desired periods of microgravity between 10 and 30 s can be achieved in aircraft flying parabolic trajectories. Although the duration and quality of these maneuvers play an important role in microgravity experiments, it is also desirable that the facility be flexible in its use and readily available on a daily basis.

To meet these demands, a study was undertaken on the potential of a small, autonomously flown unmanned aerial vehicle (UAV) as a low-cost facility for short-duration (30–40 s) microgravity experimentation. This so-called "ballistocraft for acceleration research" (BAR) should be able to fly not only preprogrammed microgravity trajectories, but partial-g trajectories as well. The possibility of partial-g maneuvers, where the specific acceleration lies in the range from 0 to $1g$, would be an additional unique and valuable feature of the BAR design, meeting the desire of scientists to simulate, for example, a Martran gravitational environment on Earth.

An important design aim was to enable very accurate microgravity maneuvers and to make the operations more independent of weather conditions such as atmospheric turbulence. Therefore a rather special design option, that of a wing that is free to rotate around a spanwise axis, was considered.

According to U.S. patent documents, the original idea of a free wing dates from before World War I. Main advantages of the free wing were expected to be increased stability, good handling qualities and stall characteristics, decreased gust sensitivity, and STOL and/or thrust-vectoring capabilities. The idea has been applied to some (very) light aircraft and UAVs with the free wing controlled by a trailing-edge flap or a "free trimmer" either in conventional or in canard configuration.[1–8]

In this paper the attitude of the wing, hinged about an axis slightly ahead of the aerodynamic center, is controlled by a torque motor. The torque motor is assumed to be capable of applying a moment about the hinge axis, that is independent of the wing deflections; that is, vibrations of the wing do not alter the applied torque. Apart from an expected decreased sensitivity to atmospheric turbulence,[1] the advantage of such a free wing could be that the aircraft would settle automatically at a certain g-setpoint, depending on the magnitude of the torque input. Moreover, the attitude of the fuselage, which will contain the payload, can be controlled independent of the attitude of the wing.

To assess the possible advantages of a free-wing craft, in particular relative to partial-gravity flight, the following issues were covered:

1) Determination of the flight characteristics of a free-wing aircraft and comparison with those of a similar fixed-wing aircraft.

2) Influence of the mechanical wing–fuselage interaction on the acceleration level of the payload.

3) Attainability of zero-g and partial-g trajectories by applying a torque to the wing.

4) Gust sensitivity of a free-wing craft compared with that of a similar fixed-wing aircraft.

To study the performance of the proposed ballistocraft, equipped with a torque-controlled free wing, and to design and test controllers for the ballistocraft, a simulation environment was set up. Because the ballistocraft flies highly nonstationary tracks with large variations of airspeed, the simulation should be nonlinear.

To increase the duration of the partial-gravity maneuvers, the trajectories should be entered with a speed as high as possible, and so it may be desirable to choose a swept-back wing to postpone compressibility effects. Each of the two wing halves would then have to rotate about its own hinge axis and have a dihedral and sweepback angle. At the same time, the two wing halves would be mechanically linked. Simulations should be able to handle this design option.

The free-wing aircraft was considered a freely moving multibody system consisting of three rigid bodies, a fuselage and two wing halves. However, both wing halves have only one degrees of freedom with respect to the fuselage and no degrees of freedom with respect to each other. As the fuselage has six degrees of freedom with respect to the inertial reference frame, the total number of degrees of freedom is seven.

To avoid the calculation of numerous reaction forces and moments in the structure of the UAV, Lagrange's equations of motion were applied to the problem, leading to the complete set of nonlinear equations of motion of a free-wing aircraft with two mechanically linked wing halves with sweepback and dihedral angle. Lagrange's equations were formulated in quasi-coordinates, leading to a set of 14 first-order differential equations.

A linear aerodynamic model was applied to the free-wing aircraft. As a first assessment of the flight characteristics of a free-wing aircraft, the equations of motion were linearized to compare the eigenmotions with those of a similar fixed-wing aircraft.

Nonlinear simulations of zero-g and partial-g trajectories flown without active control are shown. Deviations from the ideal trajectories are discussed and explained.

Finally, power spectral densities of the normal and longitudinal acceleration due to longitudinal and vertical atmospheric turbulence are shown in a simplified case to compare gust sensitivity. Also, the variances of the normal and longitudinal acceleration due to longitudinal and vertical atmospheric turbulence are determined.

II. Equations of Motion of a Free-Wing UAV

A. Reference Frames

Description of the kinematics of a free-wing airplane requires the use of at least four reference frames, one fixed to each body and one geodetic reference frame. Each reference frame is indicated by one or two characters: g, f, lw, and rw. The characters indicate the part to which the reference frame is fixed. All reference frames are right-handed. Reference frames f, rw, and lw are body-fixed (Figs. 1 and 2).

B. Notation

All transformation matrices between the different reference frames are denoted by a bold $\boldsymbol{R}$. A subscript denotes the reference frame from which a vector is transformed and a superscript denotes the reference frame to which the vector is transformed. For instance, $\boldsymbol{R}_f^g$ is the transformation matrix from the fuselage fixed axes to the geodetic axes and $\boldsymbol{R}_g^f$ is the inverse transform of $\boldsymbol{R}_f^g$.

All vectors are represented by column matrices and are printed in bold. Position vectors are named after the point of a body indicated by the vector. For example, the vector $\boldsymbol{h}$ denotes the intersection point of the hinge lines of both wing halves. The vectors $\boldsymbol{lw}$ and $\boldsymbol{rw}$ indicate the centers of mass of the left and right wing halves and the vector $\boldsymbol{f}$ indicates the position of the center of mass of the fuselage. The position vectors can be represented in different reference frames, but are always measured from the origin of the indicated reference frame. A subscript g, f, lw, or rw indicates the

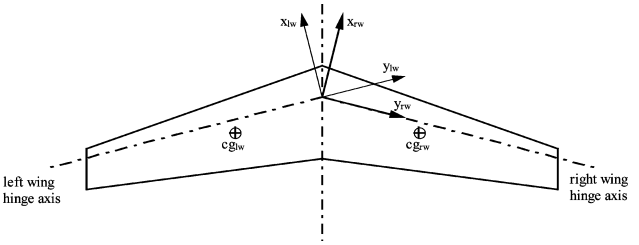

Fig. 1 Top view of left and right wing reference frames, *lw* and *rw*.

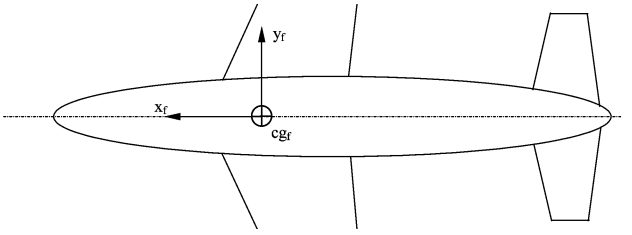

Fig. 2 Top view of the fuselage reference frame f.

reference frame relative to which the position is given. The subscript is very important in the interpretation of the vector. For instance, $\boldsymbol{h}_f$ is a constant vector, whereas $\boldsymbol{h}_g$ is not, because it depends on the attitude of the fuselage relative to the earth.

Velocity vectors and angular velocity vectors are denoted by a bold $\boldsymbol{v}$ and $\boldsymbol{\omega}$, respectively. (However, later $\boldsymbol{\omega}$ is also used to indicate a vector that contains velocity and angular velocity components of the fuselage.) A right superscript f, lw, or rw indicates the body to which the velocity applies. A left superscript denotes the reference frame in which the velocity is represented. In principle all (angular) velocities are with respect to the inertial reference frame g. For example, ${}^f\boldsymbol{v}^{\mathrm{rw}}$ is the absolute velocity of the right wing center of mass represented in fuselage fixed axes.

Skew matrices play an important role in velocity determination by means of differentiating position vectors with respect to time. When transformation matrix $\boldsymbol{R}$ is orthogonal, $\dot{\boldsymbol{R}}\boldsymbol{R}^T$ is skew-symmetric. Skew matrices will be denoted by $\boldsymbol{\Omega}$. Matrix $\dot{\boldsymbol{R}}\boldsymbol{R}^T$ will be denoted by $\boldsymbol{\Omega}$ and matrix $\boldsymbol{R}\dot{\boldsymbol{R}}^T$ by $\boldsymbol{\Omega}^T$.

The subscript in constant, time-independent vectors is omitted; that is, $\boldsymbol{h}_f$ is denoted as $\boldsymbol{h}$, and $\boldsymbol{rw}_{\mathrm{rw}}$ as $\boldsymbol{rw}$.

C. Kinematics of a Free-Wing Aircraft

The equations of motion of a mechanical system can only be determined after its kinematic properties are properly defined. In multibody dynamics the transformation matrices between local reference frames and between local reference frames and the inertial reference frame play an important role.

The position of the free-wing aircraft is defined by the position of the center of mass of the fuselage in the geodetic reference frame, given by the vector $\boldsymbol{f}_g = (x, y, z)^T$. The positions of the centers of mass of the right and left wing halves can be found as follows:

$$\boldsymbol{rw}_g = \boldsymbol{f}_g + \boldsymbol{R}_f^g \boldsymbol{h} + \boldsymbol{R}_f^g \boldsymbol{R}_{\mathrm{rw}}^f \boldsymbol{rw}, \qquad \boldsymbol{R}_f^g \boldsymbol{R}_{\mathrm{rw}}^f = \boldsymbol{R}_{\mathrm{rw}}^g$$

$$\boldsymbol{lw}_g = \boldsymbol{f}_g + \boldsymbol{R}_f^g \boldsymbol{h} + \boldsymbol{R}_f^g \boldsymbol{R}_{\mathrm{lw}}^f \boldsymbol{lw}, \qquad \boldsymbol{R}_f^g \boldsymbol{R}_{\mathrm{lw}}^f = \boldsymbol{R}_{\mathrm{lw}}^g \tag{1}$$

The attitude of the free-wing UAV as a whole is defined by the attitude of the fuselage in this paper, so all relevant parameters describing the attitude of a fixed-wing aircraft are now applied to the fuselage of the free-wing aircraft. To describe the attitude of the free-wing aircraft the standard 3–2–1 rotation sequence for the Euler angles ψ, θ, and φ is used.

The attitude of the right wing reference frame with respect to the fuselage is defined by the angles Λ_{rw}, Γ_{rw}, and θ_{rw}. Notice that angles Λ_{rw} and Γ_{rw} are constant angles defining the angle of sweepback Λ and a dihedral angle Γ of the right hinge axis with respect to the fuselage. To arrive at the attitude of the right wing half, the fuselage fixed reference frame f should be rotated about the z_f axis through an angle Λ_{rw}, about the now transformed x_f axis through an angle Γ_{rw}, and finally about the transformed y_f axis through an angle θ_{rw}, according to a 3–1–2 transformation.

To preserve geometric symmetry of the aircraft in the x_f–z_f plane, the following must hold:

$$\Lambda_{\mathrm{rw}} = -\Lambda_{\mathrm{lw}} = \Lambda, \qquad -\Gamma_{\mathrm{rw}} = \Gamma_{\mathrm{lw}} = \Gamma, \qquad \theta_{\mathrm{rw}} = \theta_{\mathrm{lw}} = \theta_w \tag{2}$$

Λ and Γ are positive angles when the hingelines are swept back and directed upward. θ_w is positive when the angle of incidence of the wing is increased.

Once the position of the center of mass of each body in the geodetic reference frame is known, the velocity for each center of mass can be determined by calculating the time derivative of the position.

For example, consider the transpose of the position vector of the right wing center of mass:

$$(\boldsymbol{rw}_g)^T = (\boldsymbol{f}_g)^T + \boldsymbol{h}^T \left(\boldsymbol{R}_f^g\right)^T + \boldsymbol{rw}^T \left(\boldsymbol{R}_{\mathrm{rw}}^g\right)^T \tag{3}$$

Because the transformation matrices are orthonormal, the inverse of each transformation matrix equals its transpose:

$$(\boldsymbol{rw}_g)^T = (\boldsymbol{f}_g)^T + \boldsymbol{h}^T \boldsymbol{R}_g^f + \boldsymbol{rw}^T \boldsymbol{R}_g^{\mathrm{rw}} \tag{4}$$

Differentiating with respect to time yields the center of mass velocity of the right wing half:

$$\begin{aligned}({}^g\boldsymbol{v}^{\mathrm{rw}})^T &= (\dot{\boldsymbol{f}}_g)^T + \boldsymbol{h}^T \dot{\boldsymbol{R}}_g^f + \boldsymbol{rw}^T \dot{\boldsymbol{R}}_g^{\mathrm{rw}} \\ &= (\dot{\boldsymbol{f}}_g)^T + \boldsymbol{h}^T \Omega_g^f \boldsymbol{R}_g^f + \boldsymbol{rw}^T \Omega_g^{\mathrm{rw}} \boldsymbol{R}_g^{\mathrm{rw}}\end{aligned} \tag{5}$$

In the derivation, use has been made of the following properties of orthogonal transformation matrices:

$$\boldsymbol{R}\boldsymbol{R}^T = \boldsymbol{I} \text{ (inverse of } \boldsymbol{R} \text{ equals its transpose)}$$

$$\dot{\boldsymbol{R}}\boldsymbol{R}^T + \boldsymbol{R}\dot{\boldsymbol{R}}^T = \boldsymbol{0} \text{ (taking the first time derivative)}$$

$$\dot{\boldsymbol{R}}\boldsymbol{R}^T + (\dot{\boldsymbol{R}}\boldsymbol{R}^T)^T = \boldsymbol{0} \text{ (transposing the second term twice)}$$

The angular velocity of the aircraft is given by three rotation components p, q, and r of the fuselage along the x, y, and z axes of the fuselage fixed axes f respectively.

Because the attitude of this body-fixed reference frame relative to the earth is given by the Euler angles ψ, θ, and φ, the angular velocity of the aircraft can also be expressed in the time derivatives of the Euler angles $\dot{\psi}, \dot{\theta}$, and $\dot{\varphi}$. The relation between rotation components p, q, and r and time derivatives $\dot{\psi}$, $\dot{\theta}$, and $\dot{\varphi}$ is given by a 3×3 nonorthogonal transformation matrix $\boldsymbol{R}_{\dot{\varphi}\dot{\theta}\dot{\psi}}^{pqr}$, whereas the rotation component of the wing halves relative to the fuselage is given by the 1×1 transformation $\boldsymbol{R}_{\dot{\theta}_w}^s = 1$, or $s = \dot{\theta}_w$.

D. Lagrange's Equations in Generalized Coordinates

The Lagrange equation is given by

$$\frac{\mathrm{d}}{\mathrm{d}t}\left(\frac{\partial L}{\partial \dot{\boldsymbol{q}}}\right) - \frac{\partial L}{\partial \boldsymbol{q}} = \boldsymbol{F}_q \tag{6}$$

The free-wing aircraft considered in this paper has seven degrees of freedom and so its position and attitude can be uniquely defined by seven generalized coordinates. The vector of generalized coordinates can be given by

$$\boldsymbol{q} = (x, y, z, \varphi, \theta, \psi, \theta_w)^T \tag{7}$$

The kinetic and potential energy of a mechanical system can be expressed in generalized coordinates and their time derivatives:

$$T = T(\boldsymbol{q}, \dot{\boldsymbol{q}}), \qquad V = V(\boldsymbol{q}) \tag{8}$$

E. Lagrange's Equations in Quasi-Coordinates

Using Eq. (6) is possible, yet not very efficient, because of the many transformations that are required to implement it. The novel and elegant solution for this problem is to find velocity components in local reference frames such as f, rw, and lw, instead of derivatives of the generalized coordinates, and to rewrite Eq. (6).

To do so, let vector $\boldsymbol{\omega}$ be defined as

$$\boldsymbol{\omega} = (u, v, w, p, q, r, s)^T \tag{9}$$

where u, v, and w are the absolute velocity components of the fuselage expressed in the fuselage fixed reference frame f along the x_f, y_f, and z_f axes, respectively; p, q, and r are the absolute angular velocity components of the fuselage expressed in the fuselage fixed reference frame f along the x_f, y_f, and z_f axes, respectively; and s is the relative angular velocity of either wing half about its hinge axis.

The kinetic energy can now be expressed as

$$\bar{T} = \bar{T}(\omega, \boldsymbol{q}) = \bar{T}(u, v, w, p, q, r, s, x, y, z, \varphi, \theta, \psi) \tag{10}$$

where $\omega = \omega(\boldsymbol{q}, \dot{\boldsymbol{q}})$.

Substitution of the expression $\bar{T}(\omega, \boldsymbol{q})$ instead of the expression $T(\boldsymbol{q}, \dot{\boldsymbol{q}})$ in Eq. (6) yields

$$\frac{\mathrm{d}}{\mathrm{d}t}\left(\frac{\partial(\bar{T} - V)}{\partial \boldsymbol{\omega}} \cdot \frac{\partial \boldsymbol{\omega}}{\partial \dot{\boldsymbol{q}}}\right) - \left(\frac{\partial(\bar{T} - V)}{\partial \boldsymbol{q}} + \frac{\partial(\bar{T} - V)}{\partial \boldsymbol{\omega}} \cdot \frac{\partial \boldsymbol{\omega}}{\partial \boldsymbol{q}}\right) = \boldsymbol{F}_q \tag{11}$$

Extensive rewriting of Eq. (11) leads to Lagrange's equations in quasi-coordinates[9]:

$$\frac{\mathrm{d}}{\mathrm{d}t}\left(\frac{\partial \bar{L}}{\partial \omega}\right)+\boldsymbol{A}\left(\frac{\partial \bar{L}}{\partial \omega}\right)-\boldsymbol{B}\left(\frac{\partial \bar{L}}{\partial \boldsymbol{q}}\right)=\boldsymbol{B}\cdot\boldsymbol{F}_q \tag{12}$$

$\boldsymbol{A}$ is a skew-symmetric matrix containing the velocity and angular velocity components of the fuselage:

$$\boldsymbol{A}=\left(\begin{array}{ccc|ccc|c} 0 & -r & q & 0 & 0 & 0 & 0\\ r & 0 & -p & 0 & 0 & 0 & 0\\ -q & p & 0 & 0 & 0 & 0 & 0\\ \hline 0 & -w & v & 0 & -r & q & 0\\ w & 0 & -u & r & 0 & -p & 0\\ -v & u & 0 & -q & p & 0 & 0\\ \hline 0 & 0 & 0 & 0 & 0 & 0 & 0 \end{array}\right) \tag{13}$$

$\boldsymbol{B}$ is a matrix containing $\boldsymbol{R}_g^f$, $\boldsymbol{R}_{\phi\theta\psi}^{pqr}$, and $\boldsymbol{R}_{\dot{\theta}_w}^s$ on its main diagonal:

$$\boldsymbol{B}=\begin{pmatrix} c\theta c\psi & c\theta s\psi & -s\theta & 0 & 0 & 0 & 0\\ -c\phi s\psi + s\phi s\theta c\psi & c\phi c\psi + s\phi s\theta s\psi & s\phi c\theta & 0 & 0 & 0 & 0\\ s\phi s\psi + c\phi s\theta c\psi & -s\phi c\psi + c\phi s\theta s\psi & c\phi c\theta & 0 & 0 & 0 & 0\\ 0 & 0 & 0 & 1 & 0 & 0 & 0\\ 0 & 0 & 0 & s\phi t\theta & c\phi & s\phi/c\theta & 0\\ 0 & 0 & 0 & c\phi t\theta & -s\phi & c\phi/c\theta & 0\\ 0 & 0 & 0 & 0 & 0 & 0 & 1 \end{pmatrix} \tag{14}$$

In Eq. (14) cosine is abbreviated to c and sine to s.

The constitution of Eq. (14) implies that $\boldsymbol{B}\cdot\boldsymbol{F}_q=\boldsymbol{F}_\omega$, because matrix $\boldsymbol{B}$ transforms $\dot{\boldsymbol{q}}$ into $\boldsymbol{\omega}$. $\boldsymbol{F}_\omega$ is the vector of generalized forces and moments acting in the directions of the degrees of freedom u, v, w, p, q, r, and s. This is a very important result, because now the aerodynamic forces can be given in the fuselage fixed reference frame f.

Because $\bar{L}=\bar{T}-V$, $\bar{T}=\bar{T}(\boldsymbol{\omega},\boldsymbol{q})$, and $V=V(\boldsymbol{q})$, Eq. (12) can finally be rewritten as

$$\frac{\mathrm{d}}{\mathrm{d}t}\left(\frac{\partial \bar{T}}{\partial \omega}\right)+\boldsymbol{A}\left(\frac{\partial \bar{T}}{\partial \omega}\right)-\boldsymbol{B}\left(\frac{\partial \bar{L}}{\partial q}\right)=\boldsymbol{F}_\omega \tag{15}$$

Equation (15) is supplemented by seven kinematic relations:

$$\dot{\boldsymbol{q}}=\boldsymbol{B}\cdot\boldsymbol{\omega} \tag{16}$$

Using Eqs. (15) and (16) offers many advantages compared to using Eq. (6). First, determining of the kinetic energy of a free-wing aircraft $\bar{T}(\boldsymbol{\omega},\boldsymbol{q})$ leads to a much simpler expression than determining the kinetic energy as $T(\boldsymbol{q},\dot{\boldsymbol{q}})$. Once kinetic and potential energy have been determined, substitution in Eqs. (15) and (16) yields a set of 14 first-order differential equations, instead of the set of 7 second-order differential equations from Eq. (6). When the equations are solved, 14 states $\boldsymbol{q}$ and $\boldsymbol{\omega}$ are found. This new approach enables the direct determination of the aerodynamic forces in body-fixed axes, which drive the equations of motion.

III. Aerodynamic Model of the UAV

The aerodynamic model used in the simulations is a linear one describing aerodynamic forces and moments during symmetric flights only. Because not much is known about the geometry of the ballistocraft yet, the model has a very general setup. Only raw geometric data such as wing area, wing span, mean aerodynamic chord, aspect ratio, and tailplane volume are used to find the aerodynamic forces and moments on the aircraft according to the work of Mulder et al.[10]

Because the free-wing aircraft is a multibody system, the center of mass of the aircraft may be moving rapidly with respect to the fuselage as the wing moves. To prevent aerodynamic derivatives from being variable, they are related to the center of mass of the fuselage instead where necessary. This can be done because the states u, v, w, p, q, r, φ, θ, and ψ are also related to the center of mass of the fuselage.

Application of a free wing has the following effects:

1) The angle of attack of the wing is a function of the angle of attack of the fuselage α and the attitude of the wing relative to the fuselage θ_w.

2) Because of the moving wing, the direction of the airflow at the horizontal stabilizer, which is influenced by the downwash of the wing, depends not only on α, but on θ_w as well.

3) In the case of a sudden change in velocity components u or w or angular velocity component q, the pressure distribution around the UAV may need a while to adjust to the new velocity state of the airplane. Only changes in angle of attack caused by a sudden change in the component w of the true airspeed along the z_f axis or caused by $\dot{\theta}_w$ will be assumed to have an unsteady aerodynamic effect. As a first approximation, the unsteady aerodynamics of the wing itself are assumed to have no effect on the wing itself.

Although the aerodynamic model is simple, it is valuable, because it provides the opportunity to compare the dynamics of a free-wing UAV to an identical fixed-wing UAV in both linear and nonlinear simulations.

IV. Results of Simulations

A. Flight Characteristics of a Free-Wing UAV

The Lagrange function $\bar{L}$ was formulated for the free-wing UAV and substituted into Lagrange's equations in quasi-coordinates (15), leading to the full set of nonlinear equations of motion. The substitution process was executed with the help of the program package Maple V Release 5. These equations of motion, which are voluminous, were then linearized around a straight stationary flight, also using Maple V. The linearized equations of motion and the aerodynamic model were implemented in a state-space form in Matlab to assess the flight characteristics.

For this first assessment of flight characteristics, the following assumptions were made: The aircraft was assumed to have two planes of symmetry, the Ox_fy_f plane and the Ox_fz_f plane. The angle of sweepback was chosen as zero and the accelerometers were placed in the center of mass of the fuselage. Furthermore, the moment coefficient about the aerodynamic center of the wing $C_{m_{\mathrm{a.c.}}}=0$. For the geometric design of the ballistocraft refer to Table 1 and Fig. 3.

These assumptions are arbitrary, but they will have an effect on the flight dynamics. Also, determining u, v, w, p, q, and r with

Table 1 Free wing geometry and mass distribution

Parameter	Value
Total mass of the UAV m	250 kg
Mass of the fuselage m_f	$\frac{4}{5}$ m
Mass of the wing halves $m_{\mathrm{lw}}=m_{\mathrm{rw}}$	1/10 m
Sweepback angle of the hinge axis Λ	10 deg
x Coordinate of the center of mass of each wing half in wing fixed axes lw or rw, w_x	$-\frac{3}{8}\bar{c}$
x Coordinate of the hingeline intersection in fuselage fixed axes, h_x	$\frac{1}{8}\bar{c}$
Distance between the aerodynamic center of the wing and the intersection of hinge axes, $x_m - x_{\mathrm{ac}}$	$-\frac{1}{8}\bar{c}$

respect to the center of mass of the fuselage does not directly give the motion of the center of mass of the aircraft as a whole. In this respect the center of mass of the fuselage is an arbitrary point.

As a nominal flight condition, a horizontal flight at sealevel with airspeed of 150 m/s was chosen.

The step response, due to an elevator deflection $\delta_e = -0.005$ rad, of a free-wing and a similar fixed-wing aircraft are compared in Figs. 4a–4d.

It can be seen that the short-period mode is well damped for the fixed-wing aircraft, but much less damped for the free-wing aircraft. Also, it has a higher frequency. The fixed-wing aircraft shows the phugoid motion, whereas in the free-wing case the phugoid is hardly excited.

Because the free-wing aircraft has one additional degree of freedom, there is another mode, a high-frequency periodic movement of the wing relative to the fuselage. This high-frequency mode is poorly damped, because of the small aerodynamic damping of the wing. However, the damping of the wing can easily be artificially increased to improve the design.

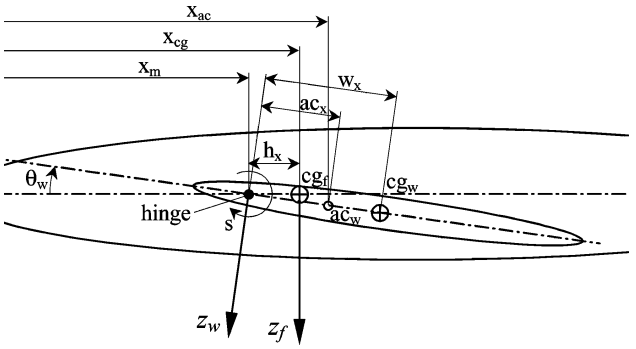

Fig. 3 Position of the hinge axis relative to the aerodynamic center of the wing.

Also, the responses of a free-wing aircraft to a stepwise increase in the wing actuator moment of 10 Nm was determined; see Figs. 5a–5d. Unlike an elevator deflection, it excites the phughoid mode of a free-wing aircraft.

B. Microgravity and Partial Gravity Flight

With the objective of flying accurate micro- and partial gravity tracks in mind, full use can be made of the free-wing concept. It is desirable that the magnitude of the specific acceleration at the payload position be constant, but also (in the case of partial gravity flight) that its direction be constant relative to the payload. This can be achieved by controlling the attitude of the fuselage (containing the payload) with the elevator, independent of the lift generated by the wing. More specifically, if the angle of attack of the fuselage is kept at 0 deg all the time, a constant force, directed perpendicular to the airflow, will generate a specific acceleration, which is constant in both magnitude ànd direction. This constant force, by definition the lift generated by the UAV, can be controlled independently by varying the moment applied about the wing hinge axis by a torque motor. Increasing the torque will rotate the wing until the moment generated by the wing lift equals the actuator moment. When the distance between the hinge axis and the aerodynamic center of the wing is approximately constant, a constant torque input will generate a more or less constant wing lift, and thus the desired specific acceleration. Of course, the engine thrust must counteract the drag at all times in this scenario. In the simulations it is assumed that sufficient knowledge of the applied engine is available to achieve effective control of the specific acceleration in the x_f direction. This study only focuses on control of the specific acceleration in the y_f direction.

With these considerations in mind, the following control strategy is chosen:

1) The elevator is used to control the angle of attack of the fuselage, thus stabilizing the short-period mode of the fuselage and providing a stabilized platform for the payload.

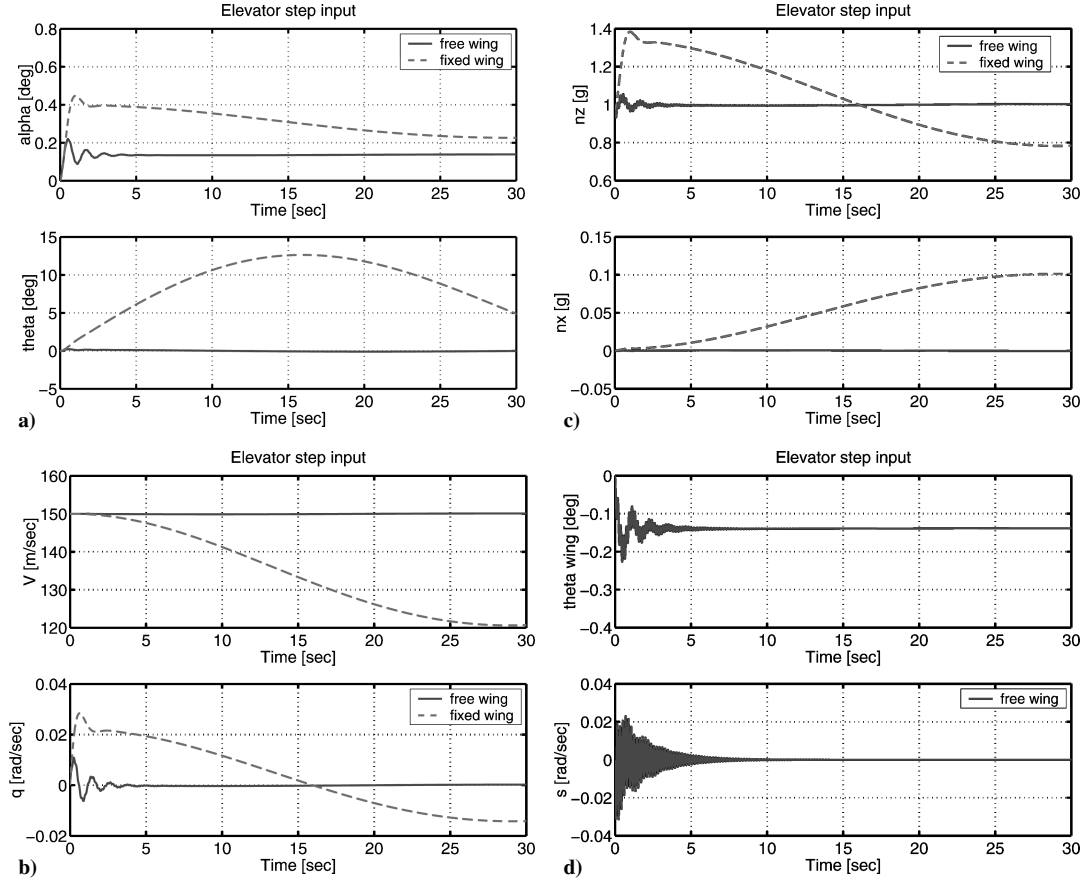

Fig. 4 Step response due to a stepwise elevator deflection (0–30 s): a) α and θ, b) V and q, c) nz and nx, and d) θ_w and s.

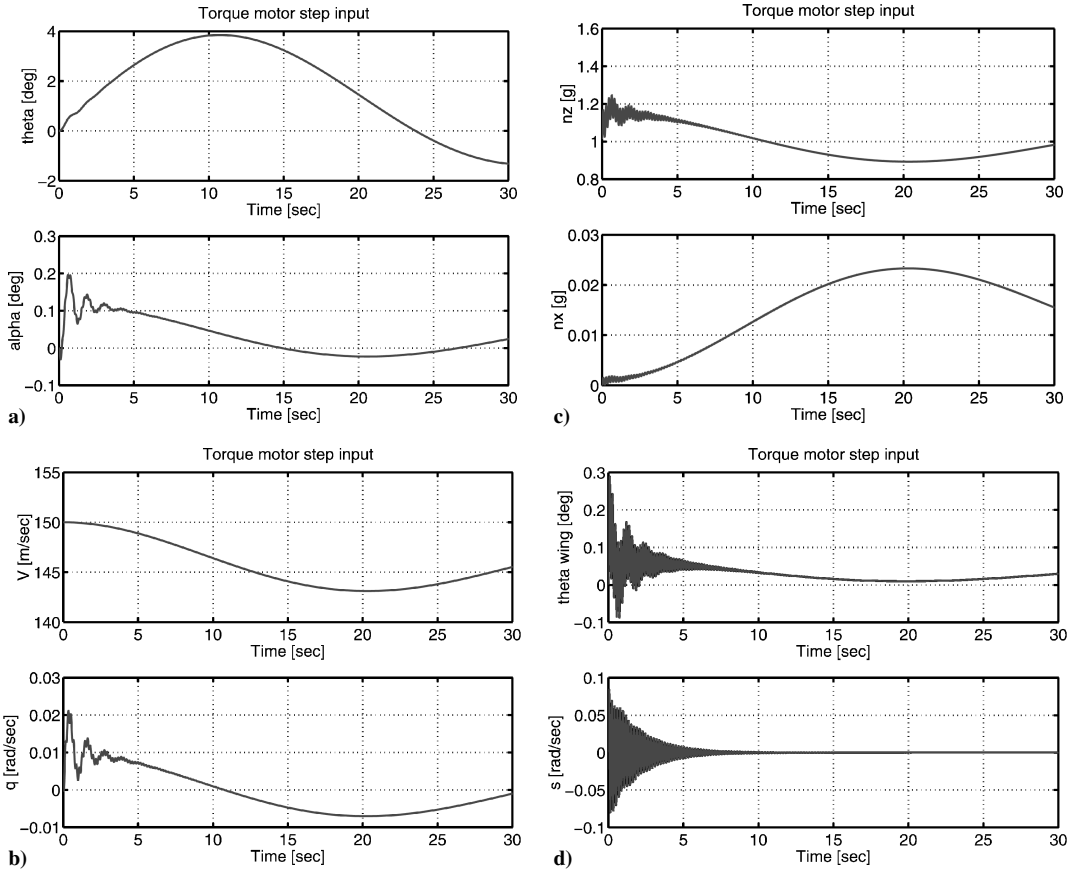

Fig. 5 Step response of due to an increase in actuator moment (0–30 s): a) α and θ, b) V and q, c) nz and nx, and d) θ_w and s.

Table 2 Designs of controllers

Feedback gains	Alpha control	Normal specific acceleration control
Proportional	$K_P = 5$	$K_P = 3\ \mathrm{Ns}^2$
Integrating	$K_I = 5\ \mathrm{s}^{-1}$	$K_I = 10$ Ns

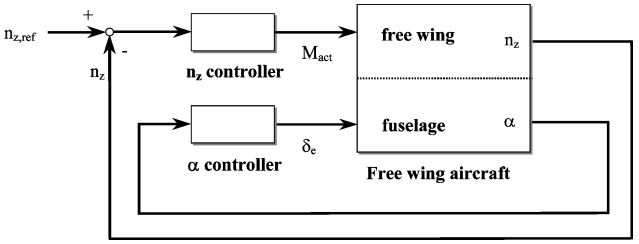

Fig. 6 Control strategy of the free-wing ballistocraft for acceleration research.

2) The moment actuator is used to control the normal specific acceleration by adjusting the angle of incidence of the free wing.

Both controllers are classic proportional integrating (PI) controllers and are designed as shown in Table 2. Refer to Fig. 6 for a graphic illustration of the control concept.

The ability of a torque-controlled free-wing aircraft to fly high-quality zero-g and partial-g trajectories with this control strategy was evaluated using nonlinear simulations of the previously used aircraft geometry. Three situations are compared: the uncontrolled UAV model, the UAV model with alpha controller keeping the fuselage angle of attack zero, and the UAV model with both alpha controller and wing torque controller aiming for the desired g-level.

Because the linear simulations showed very low aerodynamic wing damping, the damping factor has been increased by a factor of 20 by applying additional mechanical damping to the wing.

The nonlinear model was trimmed for a straight, stationary horizontal flight with fuselage angle of attack 0 deg and velocity 150 m/s, giving the following required controls and steady-state values: actuator moment $M_0 = 67.39$ Nm, elevator deflection $\delta_{e_0} = 0.02982$ rad, thrust $T_0 = 623.0$ N, and wing deflection $\delta_{w_0} = 0.02096$ rad. With these initial values the UAV was injected into a trajectory with $u_0 = 150$ m/s and $\theta_0 = \pi/3$ with thrust compensating drag and actuator moment put to zero throughout the trajectory. Although the UAV is not properly trimmed for zero-g flight, this is *deliberately* done, to show automatic settling into the zero-g flight condition.

Figure 7a shows the normal specific acceleration at the center of gravity of the fuselage with zero actuator moment and constant elevator deflection $\delta_{e_0} = 0.02982$ rad, together with the situation where the fuselage angle of attack is kept at zero using the PI controller for the elevator. It can be seen that the short-period mode damping is increased, thus reducing the settling time to the desired micro-g condition. Figure 7b shows a comparison of g-level between the fuselage angle of attack control and this same controller supplemented with the PI n_z controller for the torque moment actuator. As can be seen from the figure, an actuator moment controller is capable of increasing the micro-g quality of the maneuver. Figures 7c and 7d show the applied elevator deflection and actuator moment. Figures 7e and 7f show the effect of the different controllers on the fuselage angle of attack, respectively the wing attitude, in comparison to uncontrolled flight.

To show the capability of the UAV to achieve partial-g conditions, the aircraft is injected into a 0.38g partial gravity trajectory with $u_0 = 150$ m/s and $\theta_0 = \pi/4$, again with thrust compensating drag and actuator moment now put to 0.38×67.39 N m throughout the trajectory. Again we see an automatic settling to the desired g setpoint with increasing performance when the different controllers are applied. Figures 8a and 8b show a similar comparison between the normal specific acceleration for the 0.38g condition, as in Fig. 7, for the zero-g condition. Figures 8c and 8d show the related elevator and moment actuator activity.

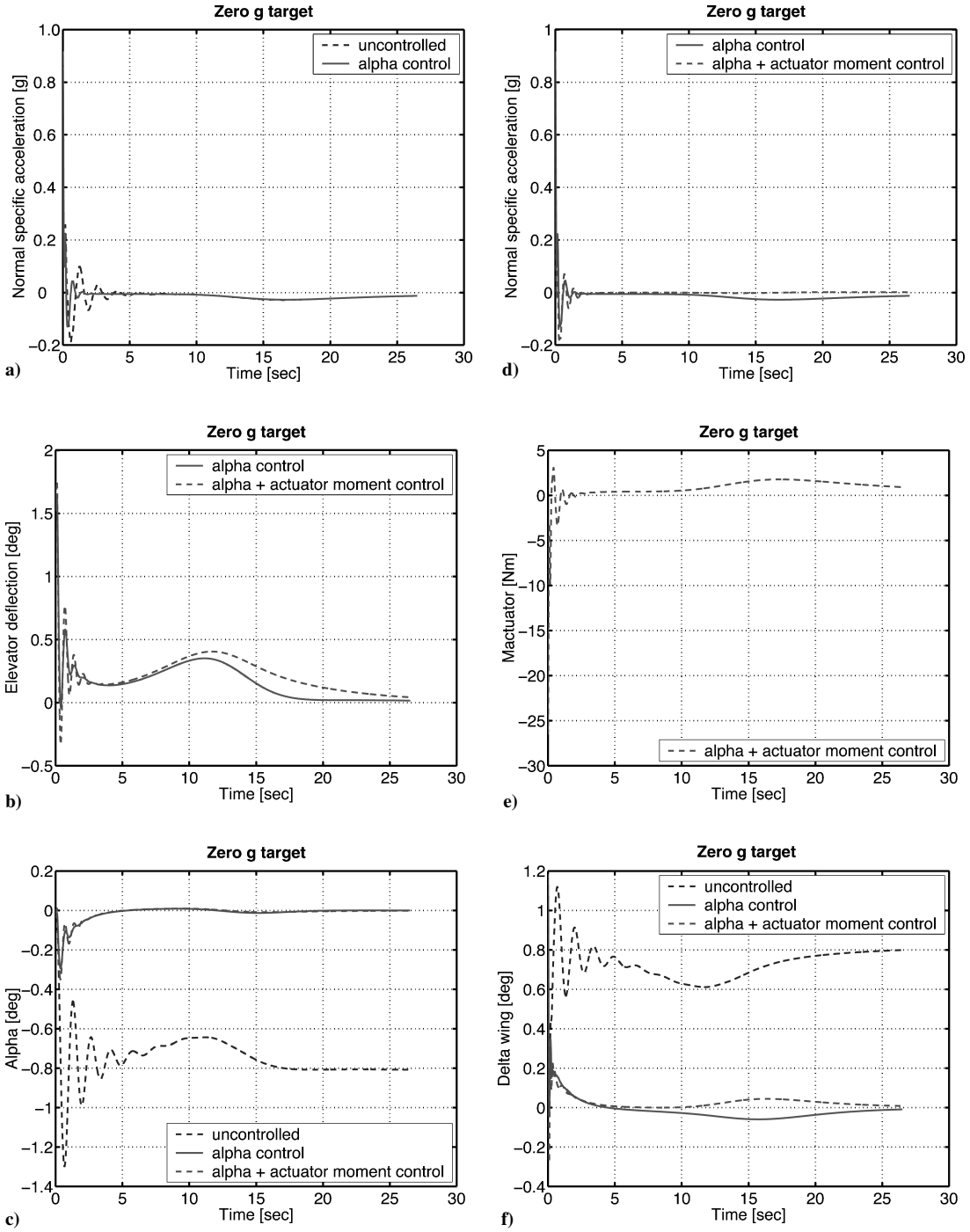

Fig. 7 Nonlinear simulation of a microgravity flight: comparison between uncontrolled flight, alpha control, and actuator moment control.

C. Gust Sensitivity

One of the presumed advantages of using a free-wing aircraft is the automatic alleviation of gust disturbances.[1] The nonlinear simulations are used to investigate this. Atmospheric turbulence is simulated using turbulence-generating filters according to the Dryden spectra, driven by white noise input.[10]

The scale length of the atmospheric turbulence is chosen as $L_{\text{gust}} = 300$ m, the variance of the gust velocities is taken as $\sigma^2 = 1\ \text{m}^2/\text{s}^2$, and true airspeed of the vehicle is 150 m/s. The atmospheric turbulence is assumed to be isotropic. Only velocity components u_{gust} and w_{gust} are generated, assuming the atmospheric turbulence is a stationary process in accordance with Taylor's hypothesis.

The UAV is trimmed for horizontal flight with speed 150 m/s and released in the turbulence field. Figure 9a shows how the wing adjusts to the airflow. The atmospheric turbulence excites the short-period mode of the aircraft, as can be seen from the realization of the angle of attack of the fuselage α_f; however, the angle of incidence of the wing δ_w adjusts to the airflow, keeping the angle of attack of the wing α_w nearly constant and resulting in a nearly constant lift. Of course the wing has its restrictions on automatically adjusting to high-frequency changes in α_w because of the inertia of the wing.

When the realizations of the normal specific acceleration of the free-wing and the fixed-wing aircraft flying through the same turbulence field are compared in Fig. 9b, the gust alleviation caused by the free wing becomes apparent. The relaxed gust response is even greater with application of the alpha controller in Fig. 9c. The related elevator control effort is shown in Fig. 9d.

To further investigate the aircraft responses to atmospheric turbulence the nonlinear model is linearized around the trimmed condition. The wind velocity components u_{gust} and w_{gust} generated by

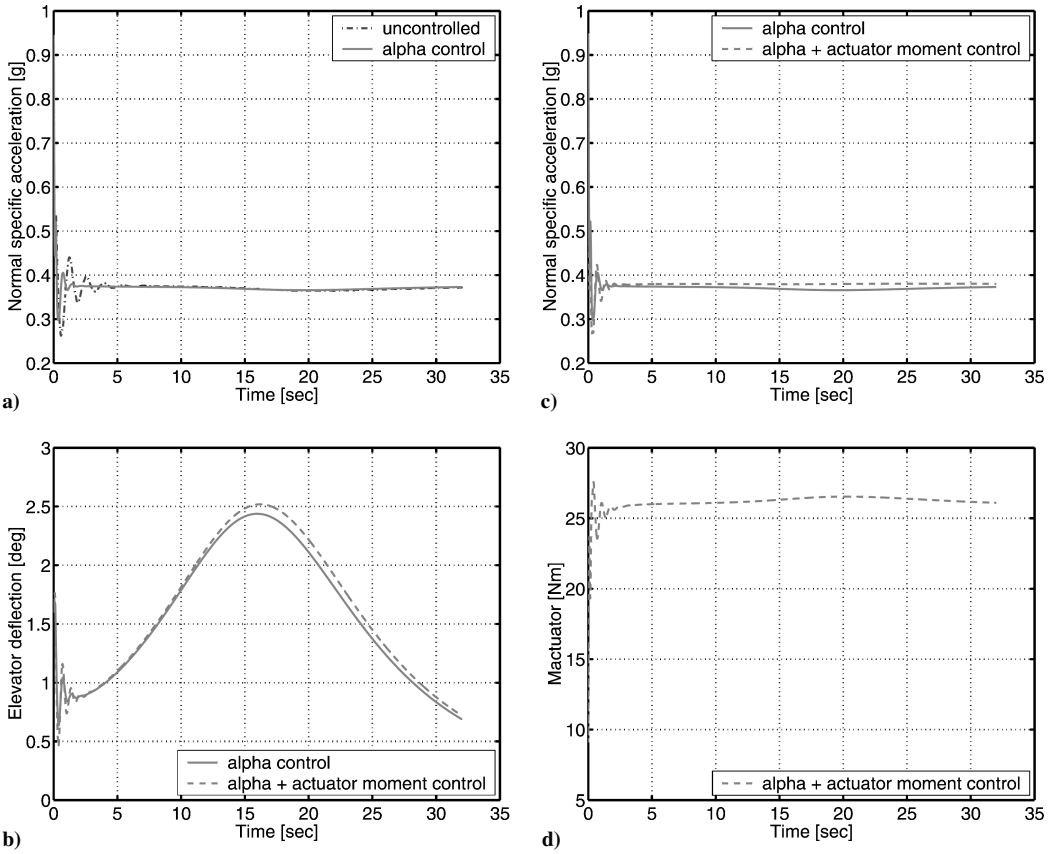

Fig. 8 Nonlinear simulation of a 0.38*g* partial gravity flight: comparison between uncontrolled flight, alpha control, and alpha + actuator moment control.

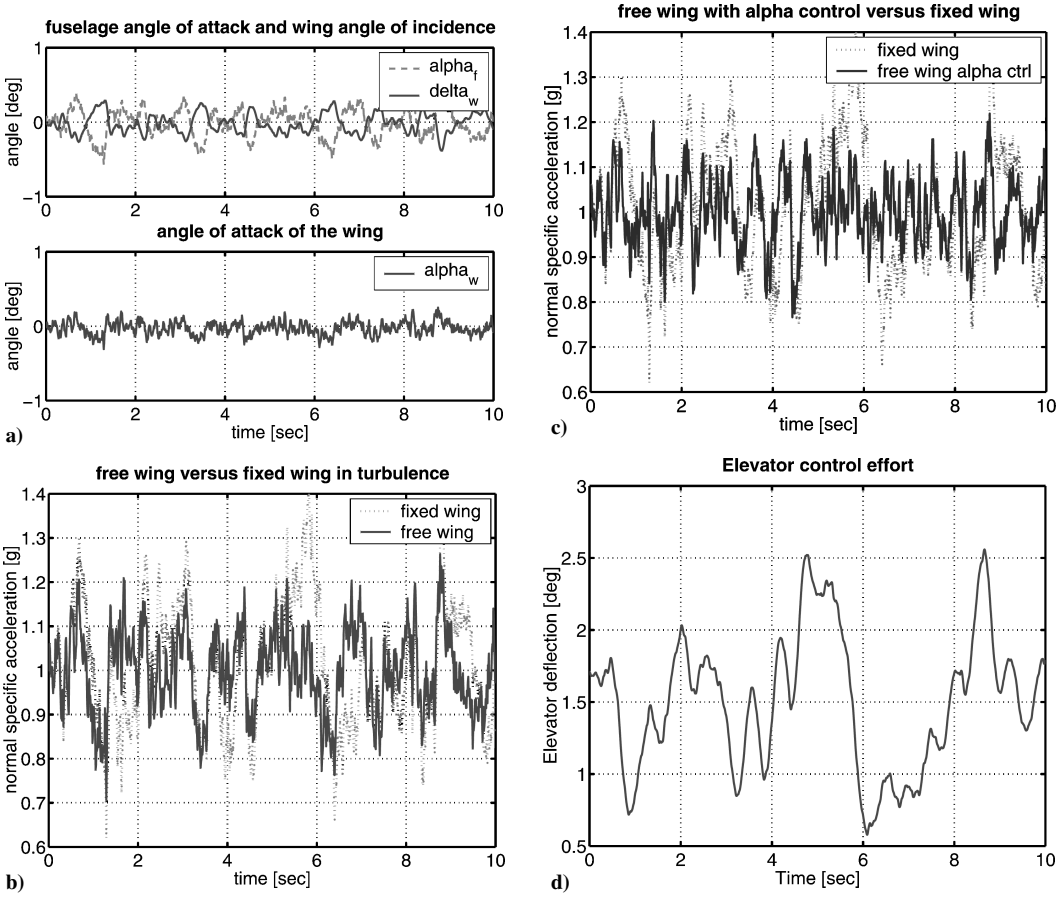

Fig. 9 Free-wing and fixed-wing UAV behavior in a turbulence field. a) The angle of attack of the fuselage and the wing deflection relative to the wing's trimmed position and the sum of both, giving the wing angle of attack: b) Normal specific acceleration of a free-wing compared to a similar fixed-wing aircraft flying through a turbulence field: c) Normal specific acceleration of a free wing with angle of attack control compared to a similar fixed wing aircraft flying through a turbulence field: d) Elevator activity associated with the angle of attack controller.

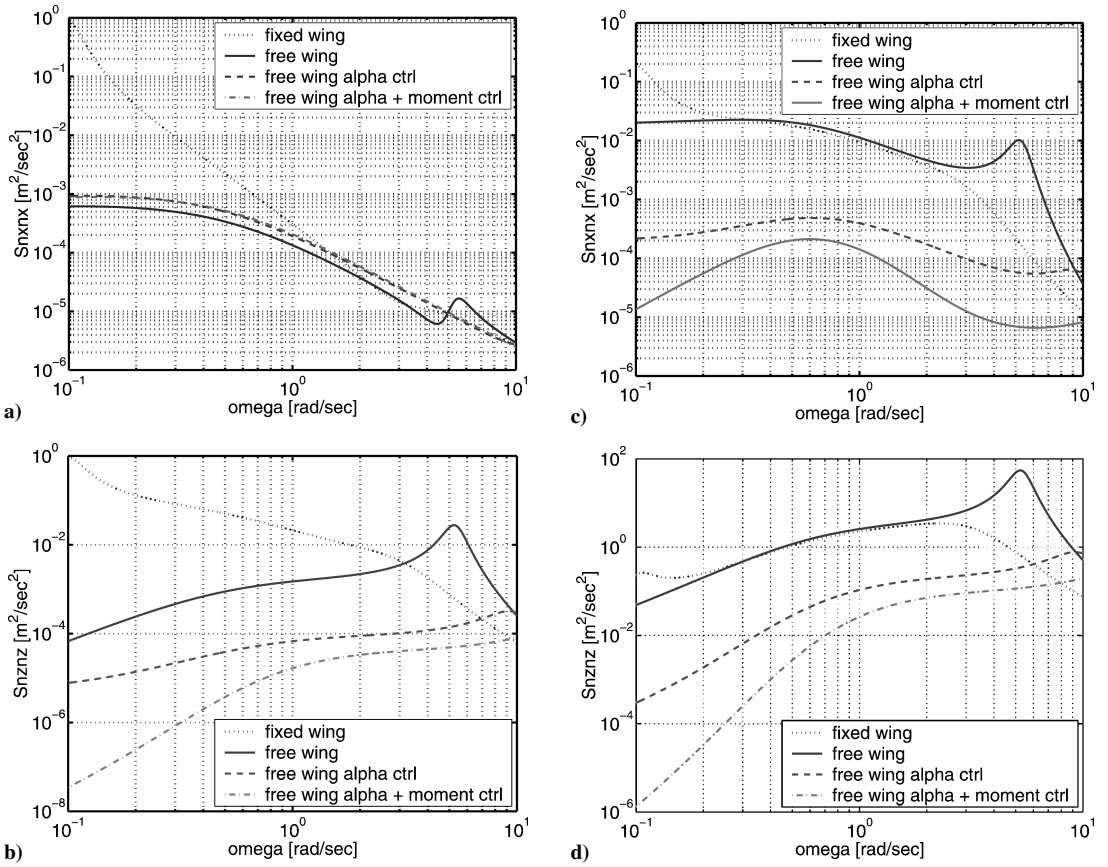

Fig. 10 Comparison of power spectral densities Sn_xn_x and Sn_zn_z related to a and b) horizontal gusts u_{gust} and c and d) vertical gusts w_{gust}.

the turbulence filters are fed into the aerodynamic model as inputs. From the transfer functions $H_{n_x u_{\text{gust}}}$, $H_{n_x w_{\text{gust}}}$, $H_{n_z u_{\text{gust}}}$, and $H_{n_z w_{\text{gust}}}$, the autopower spectral densities (PSD) $S_{n_x n_x}$ and $S_{n_z n_z}$ due to both horizontal and vertical atmospheric turbulence can be determined. The results are shown in Figs. 10a–10d. A comparison is made between the fixed-wing aircraft, the free-wing uncontrolled aircraft, the free-wing aircraft with alpha controller, and the free-wing aircraft with alpha controller ànd wing moment controller.

From the figures it can be seen that the free-wing aircraft has an advantage in gust sensitivity over the fixed-wing aircraft in the low-frequency range (lower lines on the left-hand sides of the figures). At higher frequencies the increased frequency of the short-period mode of the free-wing aircraft relative to the fixed-wing aircraft causes decreased performance of the free wing in the configuration under consideration. This negative effect can, however, be effectively suppressed by application of the alpha controller, which dampens the short-period mode of the free wing. Application of the wing moment controller reduces the gust sensitivity even more. In the high-frequency range the free-wing configuration has a disadvantage over the fixed-wing configuration because of the high natural frequency of the free wing.

It must be remarked that the PSDs depend strongly on the chosen configuration of the free wing. In this paper a more or less arbitrary choice has been made and the chosen configuration has not been optimized for, for example, position of the hinge axis, aerodynamic center of the wing, mass distribution, or hinge axis sweepback angle.

V. Conclusions

Applying a free wing to the BAR is promising as far as the simplicity of the control concept is concerned. Two relatively simply PI controllers are sufficient to fly highly accurate partial-g trajectories. Moreover, the same controllers add to a relaxed gust response of the ballistocraft. Both factors contribute to a cost-effective and flexible partial gravity facility, which can be used under different circumstances.

The design of the UAV should be optimized, using the tools presented in this paper. The configuration used in this paper is merely meant as an example to demonstrate the concept, not as a final design.

References

[1]Porter, R. F., and Brown, J. H., "Evaluation of the Gust-Alleviation Characteristics and Handling Qualities of a Free-Wing Aircraft," NASA CR-1523, April 1970.

[2]Ormiston, R. A., "Experimental Investigation of Stability and Stall Flutter of a Free-Floating Wing V/STOL Model," NASA TN-D-6831 A4088, June 1972.

[3]Wolowicz, C. H., "Free Wing Assembly for an Aircraft," *Aircraft Design, Testing and Performance*, 1978.

[4]Gee, S. W., "Flight Tests of a Radio Controlled Airplane with a Free-Wing Free-Canard Configuration," NASA TM-72853 H-1008, Jan. 1978.

[5]Porter, R. F., Hall, D. W., Brown, J. H. Jr., and Gregorek, G. M., "Analytical Study of a Free Wing/Free-Trimmer Concept," NASA CR-2946, Feb. 1978.

[6]Porter, R. F., Hall, D. W., and Vergara, R. D., "Extended Analytical Study of the Free-Wing/Free-Trimmer Concept," NASA CR-3135, April 1979.

[7]Sandlin, D. R., "Windtunnel Investigation of the Free-Wing/Free-Trimmer Concept," NASA CR-162351, Oct. 1979.

[8]Sandlin, D. R., "Windtunnel Tests of a Free-Wing/Free-Trimmer Model," NASA CR-170394, Dec. 1982.

[9]Meirovitch, L., *Methods of Analytical Dynamics*, McGraw–Hill, New York, 1970, pp. 157–160.

[10]Mulder, J. A., and Van der Vaart, J. C., "Flight Dynamics," Lecture Notes, Dept. of Aerospace Engineering, Delft Univ. of Technology, Delft, The Netherlands, Sept. 1999.